Applying reactive transport modelling in a chromium-contaminated site in the Matanza-Riachuelo basin, Buenos Aires, Argentina

Elina Ceballos* and Sergio A. Bea

CONICET-IHLLA,
República de Italia 780,
Azul, BA, C.C. 47 (B7300), Argentina
Email: eceballos@faa.unicen.edu.ar
Email: sabea@faa.unicen.edu.ar
*Corresponding author

Romina Sanci

CONICET-INGEIS,
Intendente Güiraldes 2160,
Ciudad Universitaria, CABA, (C1428EHA), Argentina
Email: romina@ingeis.uba.ar

Abstract: Chromium (Cr) is one of the main pollutants affecting both soil and groundwater systems in some areas within the Matanza-Riachuelo River Basin (MRB) in Argentina. The particular site of study is located near an abandoned tannery and chemical industry facilities. Cr toxicity and mobility depend on its oxidation state: Cr(VI) is an active carcinogen, more soluble and mobile, whereas Cr(III) shows low toxicity and solubility, precipitating in the form of amorphous $Cr(OH)_3$(am). This paper is devoted to elucidate the main key controls on the Cr(VI)-plume transport at this site using reactive transport (RT) modelling and uncertainty quantification analysis tools. RT results suggest a Cr source term on the surface to explain the observed Cr concentrations in both Pampeano and Puelche aquifers. UQ analysis indicates that the Cr(VI) concentrations in both aquifers are sensitive to hydraulic connectivity between them, the reaction reduction rates Cr(VI)-Cr(III) and the organic matter contents.

Keywords: reactive transport modelling; hexavalent chromium; groundwater; Matanza-Riachuelo river basin.

Reference to this paper should be made as follows: Ceballos, E., Bea, S.A. and Sanci, R. (2018) 'Applying reactive transport modelling in a chromium-contaminated site in the Matanza-Riachuelo basin, Buenos Aires, Argentina', *Int. J. Environment and Health*, Vol. 9, No. 1, pp.16–35.

Biographical notes: Elina Ceballos is PhD student at Geological Sciences from National University of Córdoba. She works at the Instituto de Hidrología de Llanuras 'Dr. Eduardo Usunoff' (IHLLA). Her research interests are focused on the hexavalent plume characterization in a sector of the Matanza-Riachuelo River Basin, and evaluate potential remediation strategies on the contaminated groundwater and soils.

Sergio A. Bea is an Associated Researcher at National Scientific and Technical Research Council (CONICET, Argentina). His research field is the hydrogeochemical and reactive transport modelling in the porous media. After to complete his PhD in Geology at the Technical University of Catalonia (Barcelona), he continued his specialisation in reactive transport modelling as postdoctoral fellow in the Department of Earth, Ocean and Atmospheric Sciences at the University of British Columbia, and the Earth Science Division at Lawrence Berkeley National Laboratory in both numerical issues and field applications.

Romina Sanci obtained a PhD in Geological Sciences from the Buenos Aires University. She works as Assistant Researcher of the National Scientific and Technical Research Council (CONICET, Argentina) at the Instituto de Geocronología y Geología Isotópica (INGEIS) in Buenos Aires, Argentina. Her research interests are related to the application of isotopic tracers to identify specific geochemical processes in environmental studies.

This paper is a revised and expanded version of a article entitled 'Applying reactive transport in a chromium contaminated site' presented at *AA15 II Congreso Nacional de Sociedad Argentina de Ciencia y Tecnología Ambiental y II Congreso Internacional de Ciencia Y Tecnología Ambiental*, Ciudad Autónoma de Buenos Aires, Argentina, 1–4 December, 2015.

1 Introduction

Chromium is a heavy metal that has many uses in the metallurgic, refractory, chemical and tannery industries. Chromium often occurs in the trivalent (+3) or hexavalent (+6) states under natural environmental conditions (Palmer and Wittbrodt, 1991; Rai et al., 1989). Its impact on human health depends on its redox state. Cr(VI) is more toxic and generally more mobile than Cr(III). Cr(VI) can cause perforation of the nasal septum, asthma, bronchitis, pneumonitis, inflammation of the larynx and liver and increased incidence of bronchogenic carcinoma (Kotas and Stasicka, 2000). Reversely, Cr(III) is considered to be a trace element essential for the proper functioning of living organisms. However, Cr(III) in significant concentrations can cause further adverse effects because of its high capability to coordinate various organic compounds resulting in inhibition of some metallo-enzyme systems.

The redox state, mobility and attenuation of Cr in aquifer systems are mainly controlled by the presence of minerals containing reduced forms of iron and sulphide, the presence of organic carbon-rich materials or by dispersion owing to physical mixing in the groundwater system. It is the base of the natural attenuation remediation strategy that implies the natural ability of aquifers to attenuate contaminants without intervention (e.g., see Blowes, 2002). It is a viable alternative in the site of study mainly owing to the presence of reduced forms in the sediments with the capacity to reduce Cr(VI) and the features of the groundwater system (i.e., low hydraulic gradients).

Since the beginning of the 19th century (with the settlement of the first tanneries and salteries), to the present (installation of chemical, metallurgical, electroforming industries and petroleum refineries and petrochemical facilities), the MRB has experienced a progressive degradation of water, soil and air quality. In fact, the MRB is the most

populated (>4 million people, which is 10% of Argentina's population), industrialised and polluted basin in Argentina (Zabala et al., 2016, Figure 1). Within this basin, Cr concentrations up to 5 mg L^{-1} have been detected, exceeding the permitted limit for human consumption (0.05 mg L^{-1}), established by the World Health Organization (WHO). Understanding the key issues controlling the Cr redox states in natural systems is vital for efficient management of polluted sites and the implementation of any remediation strategies.

Reactive transport (RT) modelling has become an essential tool in many disciplines within the environmental Earth Sciences (Mayer et al., 2000; Steefel et al., 2005; Bea et al., 2013). RT is used as an interpretive tool for unravelling complex interactions between coupled processes and multiple space and time scales or as a forecasting tool predicting the evolution of subsurface systems (Steefel et al., 2005; Wanner et al., 2012). This work is devoted to the application of the RT modelling in the identification of those physical and geochemical processes controlling the mobility and attenuation of Cr(VI) in the groundwater for a site into the MRB, besides evaluating the location of the potential Cr(VI) terms.

2 Site description

The area of study is located in the Jagüel, Esteban Echeverria district, into the MRB to the NE of Buenos Aires province (Figure 1(A)). It corresponds to the lowest section of Ortega stream subbasin, tributary of the Matanza River (Figure 1(B)). This subbasin covers an area of about 5500 ha with very low slopes, forming a typical plain landscape. The Ortega stream flows NNW along 10 km.

The study area has a temperate climate with warm summers, cool winters and prevailing winds from the E and NE. Average rainfall recorded at the Ezeiza station for the period 1956–2008 was 1008 mm yr^{-1} (Zabala et al., 2016). Average annual recharge is 133 mm yr^{-1} (Melián, 2014).

The population of El Jagüel is 48,000 inhabitants. In the site of study (San Ignacio neighbourhood), the population does not have access to water supply and sanitation services. The residents have their own on-site solutions through septic tanks or pits. Water supply for general uses is obtained from their private wells, while drinking water is obtained from municipal water trailer or purchase.

The area affected by Cr pollution is near two potential source terms, currently abandoned:

- a tannery (see point 1 in Figure 1(B))
- a chemical industry that manufactured Cr(VI)-salts for tanning leather (Salvador, 2013; see point 2 in Figure 1 (B)).

2.1 Hydrogeological setting

The MRB covers an area of about 2065 km^2, and it is a typical large plain basin (Figure 1(A)). It is a sedimentary basin filled up by continental and marine sediments deposited over a crystalline Precambrian basement (Zabala et al., 2016). Three different units can be defined according to their hydrogeological behaviour (Figure 2(B)). The top hydrostratigraphy unit that involves sediments of the Post-pampeano Fm. (Holocene),

formed by greyish green loessic sandy-clay silts, and sediments of the Pampeano Fm. (Pleistocene), characterised by a layer of reddish-brown, uniform and homogeneous, fine-grained loess, and red brown to green sandy loams, with few fossil remains and carbonate interbeddings (tosca). The thickness of this hydrostratigraphy unit ranges from 13 m to 70 m, and decreases in the SW-NE direction. The set of both sedimentary levels behaves as a single aquifer, which is free at the top and semi-confined at the bottom. Such an assembly is called Pampeano aquifer (termed here as PAAQ), and receives direct recharge, mainly from rainwater.

Figure 1 (A) Location of the Matanza-Riachuelo River Basin (MRB), and Ortega stream sub basin and (B) site of study, and potential Cr source terms in the Jagüel, Esteban Echeverria district

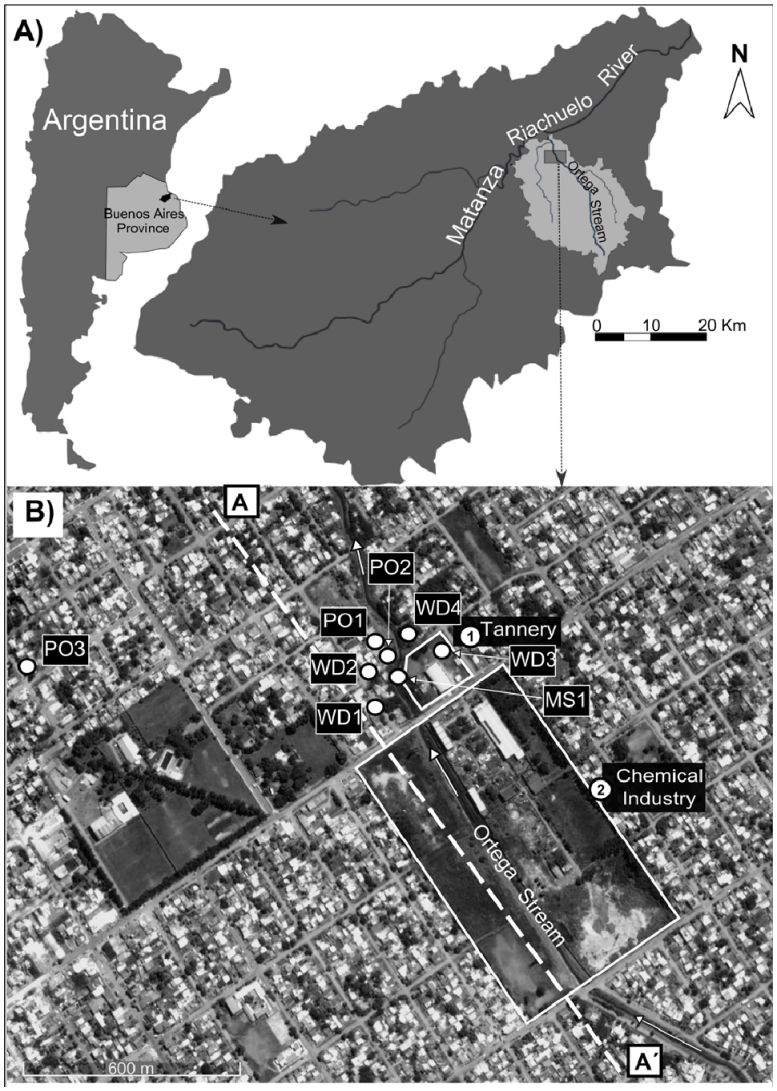

Figure 2 Reactive transport (RT) modelling: (A) modelled domain and boundary conditions for flow and solute transport; (B) hydrostraigraphic units and (C) simulated groundwater steady flow (see online version for colours)

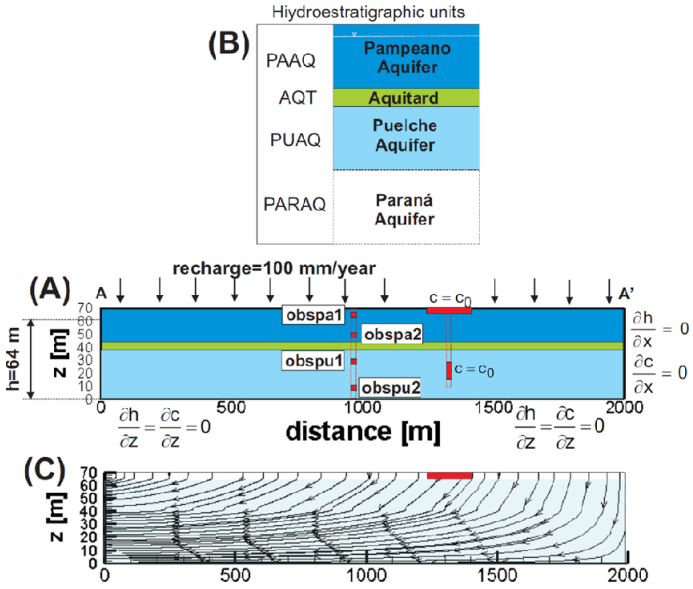

At the bottom of the PAAQ, there is a discontinuous hydrostratigraphy unit consisting of grey to greenish silty clays with variable thickness (0–13 m). It acts as an aquitard, and termed here as AQT (Figure 2(B)).

The lower hydrostratigraphy unit (Puelches Formation, Upper Pliocene to Pleistocene) is composed of yellowish brown to whitish well-sorted quartz sands, and silty clay interbeddings towards the top. It has a maximum thickness of 60 m in this region (termed here as PUAQ, Figure 2(B)). It behaves as a semi-confined aquifer. However, the hydraulic gradient favours the downward vertical flow from Pampeano to Puelche aquifer in the upstream middle part of the basin, whereas it is opposite in the lower part of the basin (Melián, 2014). The PUAQ overlies the Paraná Fm. (Miocene), consisting of confining bluish and greenish grey clays (termed here as PARAQ, Figure 2(B), it is treated as an impervious boundary).

3 Methodology

3.1 Sampling and chemical analysis

Groundwater samples were collected from three monitoring (PO1, PO2 and PO3) and four private supply wells (WD1, WD2, WD3 and WD4) located downstream from the potential Cr source contamination terms. Surface water was collected from the Ortega stream (MS1, Figure 1(B)). They were collected in high-density polyethylene bottles using dust-free gloves, and preserved in portable fridges to carry out further physicochemical analyses. Groundwater levels were measured with an electrical probe, and parameters such as electrical conductivity, temperature and pH were measured in situ

with a Multiparameter PCS Tester 35 Series. Total Alkalinity (TA) was determined by titration with H_2SO_4 0.1N. Redox couples NO_3^-, NO_2^-, NH_4^+, Fe^{+2} and total Fe were measured in situ with a portable HACH DR890 colorimeter. Major and trace element concentrations, such as total Cr, were determined at ACME LAB Bureau Veritas by ICP-MS (in the field, HNO_3 was previously added for preservation).

Groundwater chemical analytical data were interpreted through hydrogeochemical modelling using the model PHREEQC 3.0 (Parkhurst and Appelo, 2013).

3.2 Reactive transport and uncertainty quantification analysis

Reactive transport modelling was carried out with the model MIN3P (Bea et al., 2016; Mayer et al., 2002). MIN3P has been extensively verified, and used for various applications (Bain et al., 2001; Bea et al., 2012, 2016; Brookfield et al., 2006; Gerard et al., 2008; Mayer et al., 2001, 2006; Spiessl et al., 2008; Watson et al., 2003).

MIN3P solves the fluid mass conservation equation for fully saturated media given as:

$$\frac{\partial \varphi \rho}{\partial t} = \nabla \cdot \rho \mathbf{q} + \rho Q, \tag{1}$$

where $\mathbf{q}$ is the Darcy flux [L T^{-1}] defined as:

$$\mathbf{q} = -\frac{\mathbf{k}}{\mu}(\nabla P + \rho g). \tag{2}$$

ρ is the fluid density [kg m^{-3}], g is the gravity constant [m s^{-2}], φ is the porosity [–], P is the fluid pressure [kg m^{-1} s^{-2}], μ is the dynamic fluid viscosity [kg m^{-1} s^{-1}], $\mathbf{k}$ is the permeability tensor [m^2] and Q is the volumetric fluid source/sink term [m^3 m^{-3} s^{-1}].

Coupled to flow, reactive transport modelling requires solving the mass conservation equation of each chemical component according to (Mayer et al., 2002):

$$\begin{aligned} \frac{\partial \varphi T_j^a}{\partial t} &= -\nabla \cdot \left[\mathbf{q} T_j^a \right] + \nabla \cdot \left[\varphi \mathbf{D} \nabla T_j^a \right] \\ &\quad + Q_j^{a,a} + Q_j^{a,m} + Q_j^{a,e} \qquad j = 1, N_c \end{aligned} \tag{3}$$

where T_j^a are the total aqueous component concentrations [mol L^{-1}], $Q_j^{a,a}$ [mol L^{-1} s^{-1}] and $Q_j^{a,m}$ [mol L^{-1} s^{-1}] are internal source and sink terms from intra-aqueous kinetic reactions and kinetically controlled dissolution-precipitation reactions, $Q_j^{a,e}$ [mol L^{-1} s^{-1}] is an external source and sink term accounting for mass fluxes across the boundaries and $\mathbf{D}$ is the dispersion tensor [m^2 s^{-1}]. To complete the system of governing equations, an additional set of mass conservation equations has to be defined, which describes the change of mineral quantities over time (Mayer et al., 2002):

$$\frac{\partial V_{f,i}^m}{\partial t} = V_i^m R_i^m \left(\Omega_i \right), \tag{4}$$

where $V_{f,i}^m$ [–] is the volumetric fraction for the *i*th mineral species, V_i^m is its molar volume [l mol^{-1}] and R_i^m is the overall dissolution-precipitation rate for the *i*th mineral [mol L^{-1} s^{-1}] that is at the same time a function of its saturation state (Ω_i [–]). Porosity

changes owing to mineral dissolution/precipitation reactions ($\Delta\varphi^{m,t+\Delta t}$) are calculated after each time increment (Δt) as (e.g., Xie et al., 2014):

$$\Delta\varphi^{m,t+\Delta t} = \sum_{i=1}^{Nm} V_{f,i}^{m,t+\Delta t} - V_{f,i}^{m,t} \tag{5}$$

where $V_{f,i}^{m,t+\Delta t}$, $V_{f,i}^{m,t}$ are the mineral volumetric fractions for the ith mineral before and after each time increment (Δt), respectively, and N_m is the number of minerals. Total concentrations (T_j^a) in equation (3) are defined as:

$$T_j^a = c_j + \sum_{i=1}^{N_x} \nu_{ij}^x c_i^x, \tag{6}$$

where N_x are the number of aqueous complexes, ν_{ij}^x is the stoichiometric coefficient for the jth aqueous component in the ith aqueous complexation reaction, c_j is the concentration of the jth primary species and c_i^x is the concentrations of the ith aqueous complex species. Note that Ω_i (equation (4)) and c_i^x (equation (6)) are a function of the aqueous activities through the law of mass action expressions (for details see Mayer et al., 2002).

3.3 Modelling domain

The modelling domain consists of a two-dimensional vertical cross-section of about 2000 m long and 70 m deep (Figure 2(A)), oriented along the plume centreline parallel to Ortega stream inside the watershed (see line AA' in Figure 1(B)). This orientation essentially follows a groundwater streamline based on historical field data, but also predicted in a regional flow model carried out in the Matanza-Riachuelo Basin (Melián, 2014).

The three hydrostratigraphic units defined in the model consist of (Figure 2(B)):

1 the PAAQ

2 a confining AQT

3 the PUAQ.

The interfaces/thickness among the different hydrostratigraphic units within the modelled cross-section were estimated based on boreholes descriptions in the site of study and other works (e.g., Zabala et al., 2016). Homogeneous hydrogeological properties were assumed within each unit (φ = 0.1), and they are summarised in Table 1 (see base case).

3.4 Boundary and initial conditions

Impervious boundary conditions at the bottom along and the upstream vertical side of the 2D-cross section were imposed (Figure 2(A)). The last one is consistent with groundwater divides defined in the watershed based on the water-table measurements and previous numerical efforts in the area (e.g., Melián, 2014). An impervious flow boundary is also assigned at the bottom of the PUAQ, because the underlying units (Paraná aquifer) are highly clayey and continuous (Zabala et al., 2016). Estimated fluxes from rainfall records and runoff estimations are used to prescribe a fixed (average) infiltration at the

top of the modelled domain to simulate natural recharge (approximately 100 mm yr^{-1}, Melián, 2014).

In this model, the water table is not fixed a priori on the right side of the model, because it is controlled by the imposed recharge fluxes on the top (Figure 2(A)).

Initial steady-state flow conditions are computed before starting the RT simulations, imposing an initial hydrostatic pressure distribution throughout the modelled domain.

For the transport and chemistry boundary conditions, we prescribed mass fluxes based on the background chemical composition (Solution 1, Table 1), in the natural recharge, whereas the Cr(VI)-enriched waste solution composition is imposed only along the footprint of the hypothetic position of the source term on the surface (Solution 2, Table 1). Note that the Cr(VI) source term is treated here as a constant source, and it probably could be a simplification of the real system. This point will be discussed in the concluding remarks section.

Table 1 Physical and geochemical parameters considered in the Uncertainty Quantification (UQ) analysis in the Jagüel, Esteban Echeverría district (Matanza–Riachuelo Basin)

Parameter	*ID*	*Base Case*	*Range*		*Units*
			Lower	*Upper*	
Physical parameters					
Hydraulic conductivity Pampeano aquifer	k_pa	7	[1]3	[1]16	[m d^{-1}]
Hydraulic conductivity Puelche aquifer	k_pu	20	[1]17.5	[1]60	[m d^{-1}]
Hydraulic conductivity aquitard	k_aqt	10^{-5}	[1]10^{-8}	[1]10^{-2}	[m d^{-1}]
Geochemical parameters					
[2]SOC dissolution rate (k_{soc})	kin_soc	–11	–14	–8.8	$\log_{10}$ [mol L^{-1} s^{-1}]
[2]SOC percentage in volume fraction	f_soc	1	0.001	10	[%]
Cr(VI) concentrations in the source term	cr_6	24	[1]1	[1]30	[mg L^{-1}]
Initial and boundary waters					
	[3]*Solution 1* (*initial and recharge waters*)			[3]*Solution 2* (*Cr(VI)-solution*)	
pH	7.46			7.47	
CrO_4^{-2}	–			24	
$Cr(OH)_2^+$	–			–	
K^+	16.13			16.86	
[3]TIC	203.19			179.4	
Fe^{+2}	–			–	
Fe^{+3}	2.15			0.35	
Al^{+3}	4.97			0.44	
SiO_2(aq)	102.98			71.1	

[1]Melián (2014).

[2]SOC: solid organic carbon.

[3]Concentrations in [mg L^{-1}], except pH.

[4]TIC: Total inorganic carbon.

3.5 Geochemical system

The geochemical system included in the simulations was based on the observed mineralogy reported in previous works in the MRB (e.g., Zabala et al., 2016), and includes the Cr(VI)-Cr(III) species. It consists in 11 chemical components that include CrO_4^{-2}, $Cr(OH)_2^+$, H^+, Ca^{+2}, CO_3^{-2}, Fe^{+2}, Fe^{+3}, Al^{+3}, $SiO_2(aq)$, K^+ and H_2O. The included aqueous complexes are: $FeCO_3^+$, OH^-, $HSiO_3^-$, $CaOH^+$, $CaHCO_3^+$, $CaCO_3(aq)$, $AlOH^{+2}$, AlO_2^-, $HAlO_2(ac)$, AlO^+, $Al(OH)_3(aq)$, $FeOH^+$, $HFeO_2^-$, $HFeO_2(aq)$, FeO_2^-, FeO+, FeO(ac), $Fe(OH)_3^-$, $FeHCO_3^+$, $FeCO_3(ac)$, $Fe(OH)_2(ac)$, $Fe(OH)^{+2}$, $Fe(OH)_2^+$, Fe(OH)3(ac), $Fe(OH)_4^-$, $Fe_2(OH)_2^{+4}$, $Fe_3(OH)_4^{+5}$, HCO_3^-, $CO_2(aq)$, Cr^{+3}, $Cr(OH)^{+2}$, $Cr(OH)_3(aq)$, $Cr(OH)_4^-$, CrO_2^-, $HCrO_4^-$, $H_2CrO_4(aq)$, $Cr_2O_7^{-2}$, $KCrO_4^-$. The solids included in the system are the solid organic matter, $CH_2O(s)$, primary minerals as $CaCO_3(s)$ and the formation of secondary minerals as amorphous $Cr(OH)_3(am)$.

The main redox control in this geochemical system is exerted by the irreversible Cr(VI) to Cr(III) reduction induced by the organic matter contents according to the following reaction:

$$3CH_2O(s) + 4CrO_4^{-2} + 9H^+ \rightarrow 4Cr(OH)_2^+ + 3HCO_3^- + 2H_2O \qquad \text{(Reaction 1)}$$

In spite of the fact that there is no direct evidence about the occurrence of Cr(VI) to reduction, field measurements and Cr(VI)-batch experiments carried out with natural sediments suggest that it potentially could take place in this groundwater system. Note that Reaction 1 increases the groundwater alkalinity and pH. In addition, the Cr(III) concentrations owing to Reaction 1 are controlled for the formation of amorphous $Cr(OH)_3(am)$ (reversible reaction) according to:

$$Cr(OH)_3(am) + H^+ \leftrightarrow Cr(OH)_2^+ + H_2O. \qquad \text{(Reaction 2)}$$

Carbonate dissolution is assumed to exert the pH buffer control in this system according to:

$$CaCO_3(s) + H^+ \leftrightarrow Ca^{+2} + HCO_3^-. \qquad \text{(Reaction 3)}$$

Cr(VI) reduction rates for Reaction 1 were simulated according to a zero-order kinetic expression when the Cr(VI) concentrations are in excess, and a first-order expression close to a monod constant $k_{1/2}$ (Mayer et al., 2001):

$$R_{CH2O-Cr} = k \cdot [Cr(VI)] \cdot \left(\frac{[CH_2O(s)]}{k_{1/2} + [CH_2O(s)]} \right). \qquad (7)$$

In addition, the minerals $CaCO_3(s)$ and $Cr(OH)_3(am)$ (Reaction 2) were considered in equilibrium, and their dissolution/precipitation rates were modelled with the following kinetic expression:

$$R = k_{eff} \left(1 - \frac{IAP}{K} \right) \qquad (8)$$

where R is the reaction rate [M L^{-1} s^{-1}], k_{eff} is the kinetic constant [M L^{-1} s^{-1}], IAP is the ionic activity product and K is the equilibrium constant.

Volumetric fractions for carbonates ($CaCO_3(s)$) and organic matter contents ($CH_2O(s)$) for all units were 0.09 and 0.008, respectively.

3.6 Modelling scenarios

Two different scenarios (identified here as base cases) were simulated based on the hypothetical location of the Cr(VI) source terms. As regards the first one (Scenario I), a Cr(VI) source term on the surface is simulated (see Figure 2(A)). As regards the second one (Scenario II), the injection of Cr(VI)-enriched waste water into the deep aquifer (i.e., PUAQ) is simulated (see Figure 2(A)). The main physical and geochemical model parameters for the base case simulations are shown in Table 1. They were chosen according to the best fit of the chromium concentrations, and these values are in the range of parameter values reported in the literature. The total simulated period of time was about 100 years, starting from 1960, when the activities of the near chemical facilities were starting (Salvador, 2013).

3.7 UQ approach and methodology

Uncertainty quantification (UQ) analyses were conducted to evaluate the model result sensitivity to important input parameters and the effect of parameter uncertainty on the predicted migration of the Cr(VI) plume. The UQ toolset developed in ITOUGH2 (Finsterle, 2010) was applied in this study. Details on the sensitivity analysis method implemented in ITOUGH2 and the approach followed for the UQ analyses are presented in the following section (for reference, see also Bea et al. (2013)).

In this study, ITOUGH2 was coupled with the MIN3P code, using the PEST protocol (Doherty, 2008) as a pre- and post-processor for sampling the MIN3P input parameter values and analysing the simulation outputs. ITOUGH2 includes several parameter sensitivity methods. The method used in this study is the Morris one-at-a-time (OAT, Morris, 1991).

Parameter sensitivity is commonly defined as a partial derivative of the change of the output variable caused by a unit change in each parameter from reference values (Bea et al., 2013; Cacuci, 2003). This is referred to as a local sensitivity approach, because it is dependent on a set of reference parameter values, unless the system is perfectly linear. In the Morris OAT method, the calculated partial derivative is called the 'elementary effect', and for the case of the *i*th parameter (EE_i), it is computed as:

$$EE_i = \frac{\left(y\left(p_1,...,p_{i-1},p_i+\Delta_i,p_{i+1},...,p_k\right)-y\left(\mathbf{P}\right)\right)}{\Delta_i}, \tag{9}$$

where $\mathbf{P} = (p1, \ldots, pk)$ is a vector of k parameter values, $y(\boldsymbol{P})$ is the output of the model for the parameter vector $\boldsymbol{P}$ and Δ_i is the increment in the ith parameter such that $p_i + \Delta_i$ is still in the range of allowable values.

A number of 70 simulations covered the range of uncertainties of three flow parameters (the permeability for each hydrogeological unit and the AQT) and three geochemical parameters (Cr(VI) concentrations in the source term, the Cr(VI)-Cr(III) reduction rate and organic matter contents). These uncertainty ranges were based on those reported in the literature (e.g., Jamieson-Hanes et al., 2012; Melián, 2014), and they are tabulated in Table 1.

4 Results and discussion

A summary of the results from the chemical analysis of groundwater and superficial water samples is shown in Table 2. It shows that groundwater samples contain high dissolved Cr concentrations. The highest value of total Cr (5.6 mg L^{-1}) was observed on the top of the deeper aquifer (PUAQ in Figure 2(B)), and corresponds to the private supply well (WD1) located downstream near the chemical factory (Figures 1(B) and 3(A)). On the other hand, the private supply wells (WD3 and WD4), near the old tannery installations, show Cr concentrations around 0.01 mg L^{-1}, suggesting the chemical industry as the potential source term.

In the site of study, groundwater pH ranges from 7.12 to 8.13, suggesting neutral to alkaline conditions. Spatial distribution of the Stiff diagrams for the different groundwater samples is shown in Figure 3(B). Generally, groundwater samples are Na-HCO_3 type, but some of them increase their Cl, SO_4 and Na contents, particularly those ones near the chemical factory (see samples WD1 and WD2 in Figure 3(B)), with the major Cr contents (see samples WD1 and WD2 in Figure 3(A)). It is clearly evident in a Cr vs. $Ca/(Ca + SO_4)$ plot (Figure 4), and it suggests an additional SO_4 source, probably linked to the Cr one. In this figure, samples could be grouped as:

1 with low SO_4 and Cr contents

2 with major SO_4 and Cr contents.

Redox potentials of water were calculated with the Nernst equation using the NO_3^-/NO_2^- couple, and they are tabulated in Table 2, and plotted in both pH-pe diagrams for Cr and N_2 species, respectively (Figure 5). As regards the pH-pe diagram for Cr species (Figure 5(A)), water samples fall in the CrO_4^{-2} stability field [Cr(VI)], close to the boundary of the $Cr(OH)_3$(am) field [Cr(III)]. It suggests that Cr(VI) is being reduced to Cr(III). As regards the pH-pe diagram for N_2 species (Figure 5(B)), groundwater samples fall mainly in the NO_3^- field. These results suggest oxidising conditions, and they are consistent with the Cr(VI) redox state, but Cr(III) concentrations should be controlled by the precipitation of Cr $(OH)_3$(am). Mineral saturation indexes calculated with the model PHREEQC show these groundwater samples are close to equilibrium with this mineral (results shown in Table 2).

Lastly, hydraulic gradients observed between monitoring wells PO1 and PO2 (Table 2) show an important downward vertical component in the groundwater flow from the upper (PAAQ) to the lower aquifer (PUAQ).

4.1 Groundwater flow modelling results

The water-table position and flow streamlines under steady state are shown in Figure 2(C). Groundwater flow was driven not only through the PAAQ, but also through the PUAQ. Despite the low permeability of the AQT unit, leakage from the PAAQ to the PUAQ is predicted to take place over most of the flow domains. As was described earlier, it is consistent with the piezometric measurements in both aquifers (Table 2), and those ones reported in the literature for other zones in the same basin (Zabala et al., 2016). This last result could imply an important issue in the migration of the Cr(VI) plume from the surface to deep portions of the aquifers (Figure 6(A)).

Table 2 Chemistry compositions of groundwater and surface water samples and saturation indexes of $Cr(OH)_3$ (am) mineral phase

Name	*Well depth* m	*WT*[©] m	*Aquifer*	*pH*[©]	*pe**	*EC*[©] µS/cm	*TA*[©] ppm $CaCO_3$	NO_3[©] ppm	NO_2[©] ppm	*Ca* ppm	*Mg* ppm	*Na* ppm	*K* ppm	*Cl* ppm	SO_4 ppm	*Cr* ppm	*SI* $Cr(OH)_3$(am)
PO1	15	2.6	Pampeano	7.12	7.86	1384	463	67.2	10	88.3	40.4	198.8	21.3	89	93	0.13	–0.09
PO2	40	4.4	Top of Puelche	7.63	7.27	1267	429	59.9	12	45.4	25.0	243.8	13.5	98	84	1.33	0.38
PO3	20	5.9	Pampeano	7.41	7.53	1424	508	69.4	12	64.8	38.3	257.5	16.1	74	39	0.005	–1.24
DW1	30	–	Top of Puelche	7.51	7.54	2180	373	110.1	11	85.1	43.8	325.7	16.8	256	198	5.63	1.61
DW2	15	–	Pampeano	7.6	–	1386	429	NM	NM	57.5	29.5	252.7	14.4	83	108	0.45	–0.04
DW3	15	–	Pampeano	7.33	7.85	1810	693	64	6	48.4	58.3	245.2	25.5	91	138	0.02	–0.72
DW4	15	–	Pampeano	8.13	–	1481	454	NM	NM	72.9	47.2	234.6	22.2	109	102	0.01	–5.55
MS1	arroyo	–	–	8.11	6.38	900	395	98.3	47	28.5	9.2	168.3	16.0	51	18	0.001	–6.68

WT: water teable; *: calculated based on Nernst equation from NO_3^-/NO_2^- redox cuple; EC: electrical conductivity; TA: total alkalinity; [©]field measured; NM: not measured; (SI): mineral saturation indexes.

Figure 3 (A) Spatial distribution of Cr plume in the neighbourhood San Ignacio, El Jagüel, Esteban Echeverria district (in mg L^{-1}). (B) Stiff diagrams for groundwater and surface water samples in the site of study

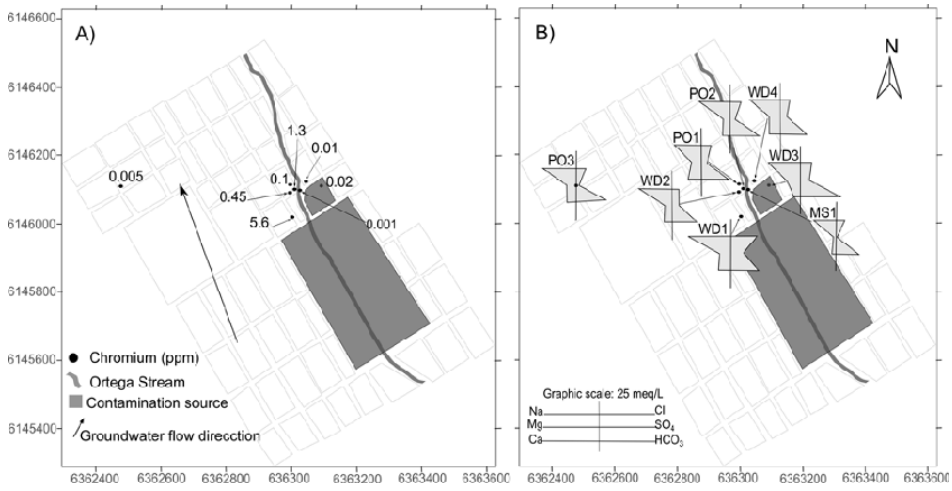

Figure 4 Cr concentrations (mg L^{-1}) vs. Ca/(Ca+SO_4) (molar) in groundwater and surface water samples collected in the neighbourhood San Ignacio, El Jagüel, Esteban Echeverría district (see online version for colours)

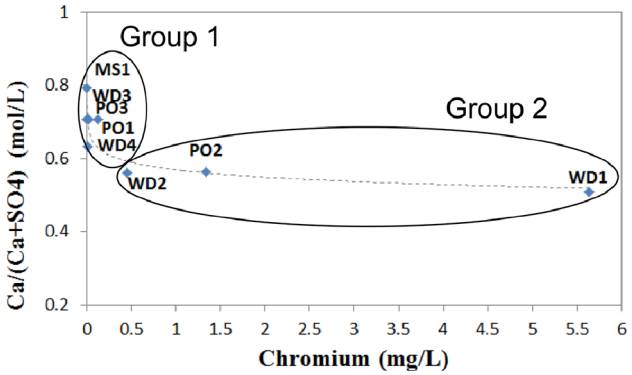

4.2 Base case simulation: scenario I (Cr(VI) source term on the surface)

In this scenario, the modelling results suggest the formation of at least two Cr concentration plumes. The first one is forming into the PAAQ unit, whereas the second (and main one), in the PUAQ unit (Figure 6). These results could explain the observed presence of Cr concentrations in both aquifers (see Cr concentrations in Table 2). However, it mainly depends on the hydraulic connectivity between both aquifers through the AQT unit.

Cr(VI) concentrations are transported downstream from the source term predicting a maximum of 8 [mg L^{-1}] in the upper part of the PUAQ (Figure 7(E)), whereas a maximum of almost 4 [mg L^{-1}] in the bottom of the PAAQ (Figure 7(C)).

Figure 5 pH-pe diagrams for (A) Cr, and (B) N_2 species (see online version for colours)

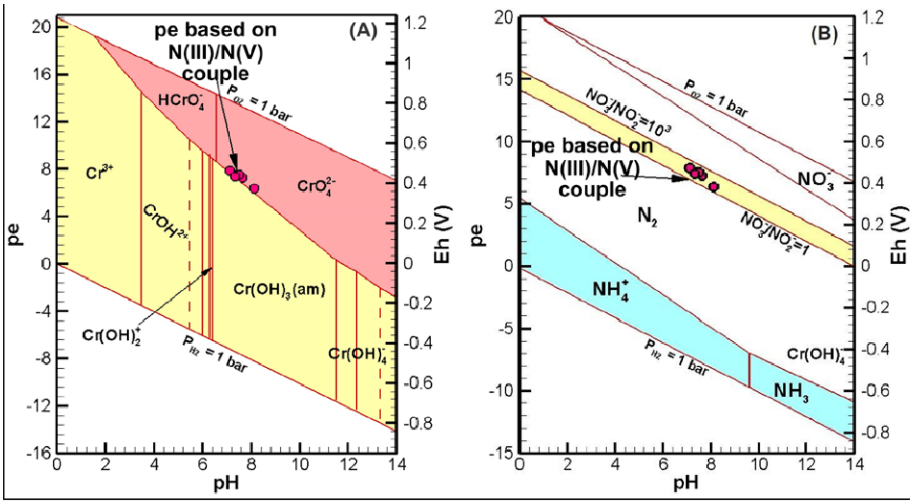

Figure 6 Reactive Transport (TR) modelling results for base case simulation (Scenario I): (A) Cr(VI) concentrations at 10, 50 and 100 years of simulation; (B) Cr(III) concentrations at 10, 50 and 100 years of simulation; (C) saturation index for $Cr(OH)_3(am)$ at 10, 50 and 100 years of simulation and (D) volumetric fraction for $Cr(OH)_3(am)$ at 10, 50 and 100 years of simulation (see online version for colours)

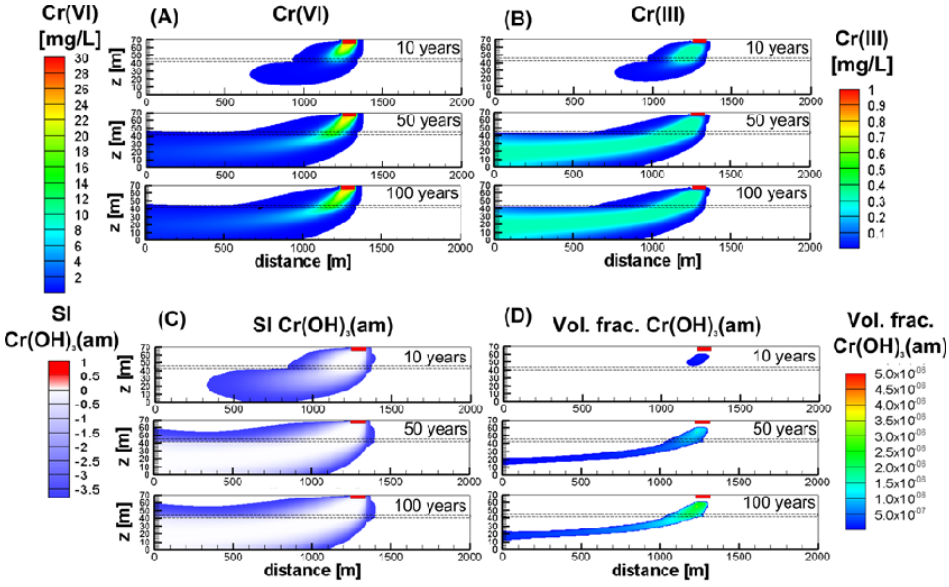

As a consequence of the Cr(VI) reduction induced by the organic matter contents, Cr(III) concentrations raise (and not exceed) 0.3 [mg L^{-1}] in the bottom and upper parts of the Pampeano and Puelche aquifers, respectively (Figure 7(C) and (E)). Cr(III) concentrations are controlled by equilibrium with $Cr(OH)_3(am)$ (see Figure 6(C) and (D), and Figure 7(C) and (E)).

A variant on this scenario was simulated decreasing the AQT hydraulic conductivity. In this case, practically the Cr plume is forming into the PAAQ, and the maximum Cr(VI) concentrations raise to 8 [mg L^{-1}] in the shallow part of it. Note that the groundwater flow simulated in this scenario variant cannot explain the Cr concentrations observed in the PUAQ (Table 2).

Figure 7 Reactive transport (TR) modelling results for base case simulations. Temporal evolution for the Cr(VI) and Cr(III) concentrations, and saturation index for $Cr(OH)_3(am)$. (A), (C), (E) and (G) temporal evolution in observation points (see Figure 2(A)) obspa1, obspa2, obspu1 and obspu2, respectively for Scenario I. (B), (D), (F) and (H) temporal evolution in observation points (see Figure 2(A)) obspa1, obspa2, obspu1 and obspu2, respectively for Scenario II

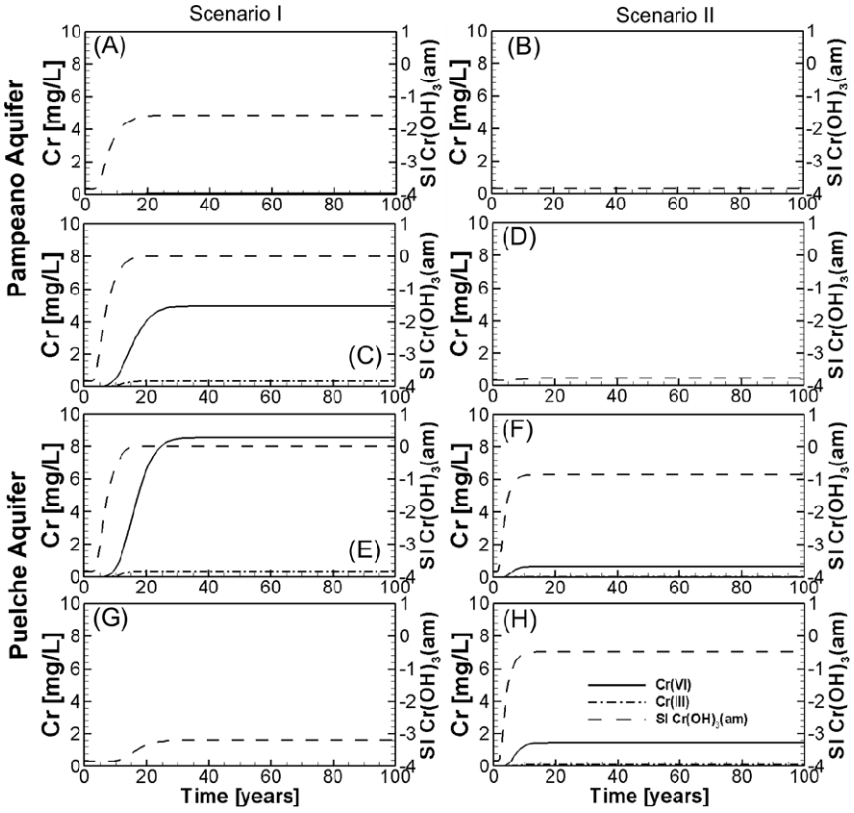

4.3 Base case simulation: scenario II (injection of cr(VI)-enriched waste water)

This scenario simulates the direct injection of Cr(VI)-enriched waste solutions into the deep aquifer (PUAQ, Figure 8(A)). It was motivated:

1 by the presence of important Cr(VI) concentrations in this aquifer in the site of study

2 because was suggested as a common practice in other contaminated hydrogeological systems (e.g., see Economou-Eliopoulos et al., 2011).

Cr plume is only forming into the PUAQ (Figure 8(A) and (B)), and this scenario cannot explain the observed Cr(VI) concentrations in the upper aquifer (PAAQ, Table 2).

Figure 8 Reactive transport (TR) modelling results for base case simulation (Scenario II): (A) Cr(VI) concentrations at 10, 50 and 100 years of simulation; (B) Cr(III) concentrations at 10, 50 and 100 years of simulation; (C) saturation index for $Cr(OH)_3(am)$ at 10, 50 and 100 years of simulation and (D) volumetric fraction for $Cr(OH)_3(am)$ at 10, 50 and 100 years of simulation (see online version for colours)

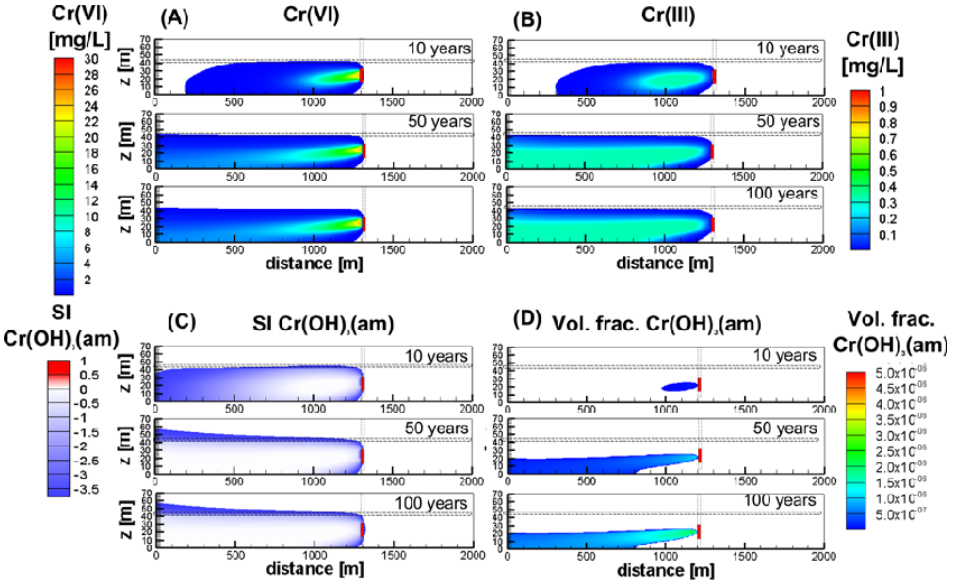

4.4 UQ analysis results

To investigate the impact of variable flow and uncertain geochemical parameters on the Cr(VI) plume migration, we choose to examine predicted Cr(VI) concentrations at several modelled observation locations aligned along a hypothetical borehole at 800 m downstream of the hypothetical Cr(VI) source term (Figure 2(A)):

1 two locations in the upper and lower part of the PAAQ (obspa1 and obspa2, respectively)

2 two locations in the upper and lower part of the PUAQ (obspu1 and obspu2, respectively).

4.5 UQ analysis results (Scenario I)

The temporal evolution of the mean EE for Cr(VI) concentrations is shown in Figure 9. This figure shows that the predicted Cr(VI) concentrations are sensitive to different flow and geochemical input parameters, and also this sensitivity evolves in the space (vertical) and time.

As regards the sensitivity of Cr(VI) concentrations to physical parameters in the PAAQ, as would be expected, they are mainly sensitive to the hydraulic conductivities of the aquitard (*k_aqt*) unit, and slightly sensitive to Pampeano (*k_pa*) and Puelche (*k_pu*) hydraulic conductivities (e.g., see OBSPA2 in Figure 9(C)). However, these sensitivities are different among them. For instance, it is negative to *k_pu* because Cr(VI) concentrations decrease as the leakage between Pampeano and Puelche aquifers increases

as a consequence of increments in hydraulic conductivity in the PUAQ. On the other hand, the sensitivity to *k_pa* is positive because increments in Pampeano hydraulic conductivities imply that the Cr(VI) plume is practically forming in this aquifer (Figure 9(C)).

Figure 9 Results for the UQ (Uncertainty Quantification; OAT, Morris, 1991) analysis for both Scenarios: (A) Scenario I: It considers a Cr(VI) source term on the surface and (B) Scenario II: It considers the direct injection of Cr(VI)-enriched waste water into the Puelche aquifer (see online version for colours)

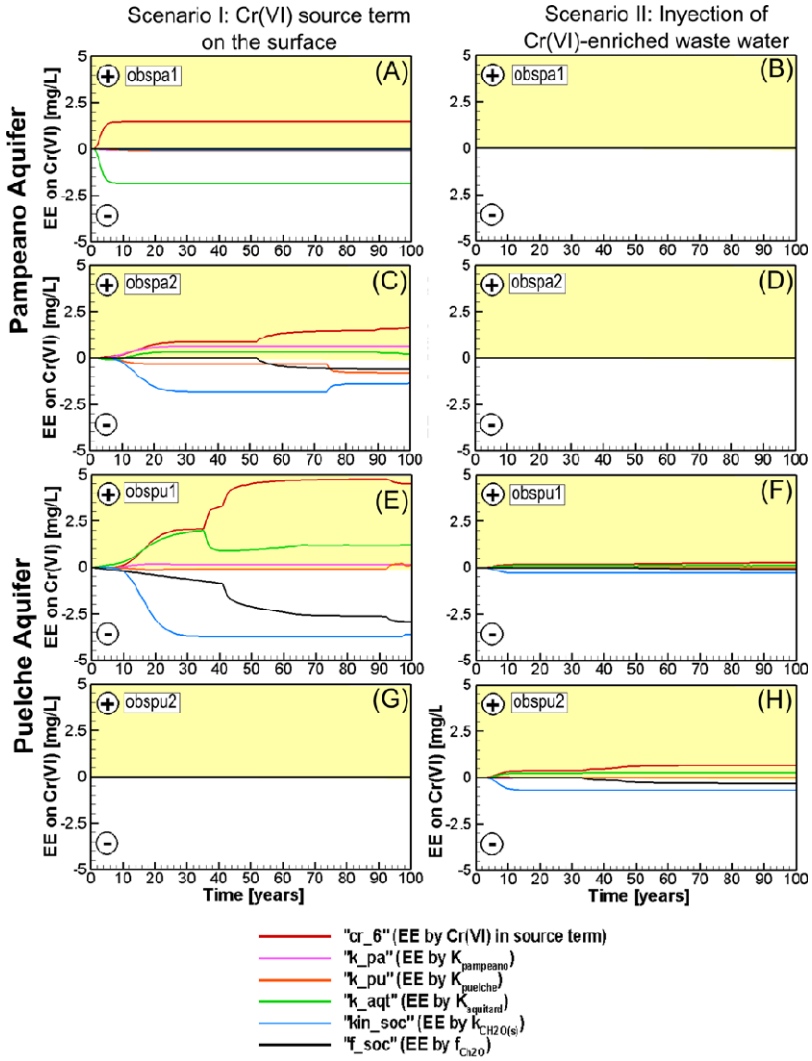

EE: elementary effect.

As regards the sensitivity of Cr(VI) concentrations to geochemical parameters in the PAAQ, they are strongly sensitive to Cr(VI) concentrations in the source term (*cr_6*), the reduction Cr(VI)-Cr(III) rates (*kin_soc*) and the organic matter contents (*f_soc*) (Figure 9(C)). Again, their behaviours are also different among them. Cr(VI)

concentrations show a positive sensitivity when Cr(VI) load increases. However, Cr(VI) concentration sensitivities are negative to reduction rates (*kin_soc*) and organic matter contents (*f_soc*) because both parameters increase the Cr(VI) to Cr(III) reduction rates.

As regards the sensitivity of Cr(VI) concentrations to physical parameters in the PUAQ (see obspu1 in Figure 9(E)), they are also sensitive to the aquitard hydraulic conductivity (*k_aqt*) but with an opposite behaviour than in the PAAQ (compare this parameter in obspa2, Figure 9(C)). In this case, this sensitivity is positive because Cr(VI) concentrations increase as the leakage between Pampeano and Puelche aquifers increases.

As regards the sensitivity of Cr(VI) concentrations to geochemical parameters in the PUAQ, they are sensitive to Cr(VI) load (*cr_6*), the reduction Cr(VI) to Cr(III) rates (*kin_soc*) and the organic matter contents (*f_soc*) (Figure 9(E)). It is positive for the first one because Cr(VI) concentrations increase with the Cr(VI) load, but they are negative for the last two ones because Cr(VI) concentrations decrease when the reduction Cr(VI) to Cr(III) rates increase.

4.6 UQ analysis results (Scenario II)

For this scenario, the temporal evolution of the mean EE for Cr(VI) concentrations is shown in Figure 9. Cr(VI) concentrations are only sensitive in the PUAQ but in a lesser extent than in Scenario I. This sensitivity also evolves in the space (vertical) and time.

Cr(VI) concentrations are mainly sensitive to geochemical parameters in the observation point in the bottom of the aquifer (see obspu2 in Figure 9 (H)). They are sensitive to Cr(VI) load (*cr_6*) and the reduction Cr(VI) to Cr(III) rates (*kin_soc*). It is positive for the first one because Cr(VI) concentrations increase with the Cr(VI) load, but they are negative for the last one because Cr(VI) concentrations decrease when the reduction Cr(VI) to Cr(III) rates increase.

5 Concluding remarks

Reactive transport (RT) is used here as a numerical tool to assess a groundwater system contaminated with Cr in the Matanza-Riachuelo Basin (in the El Jagüel, Esteban Echeverría district). Here, redox potentials based on NO_3^-/NO_2^- couple show oxidation conditions, Cr(VI) being the dominant oxidation state. This is consistent with the high dissolved groundwater Cr concentrations observed in the site of study (>5 mg L^{-1}).

Cr measurements and RT modelling results suggest that a Cr source term on the surface is the most realistic scenario to explain Cr concentrations in both Pampeano and Puelche aquifers. They show that at least two Cr plumes are forming in both aquifers and they are transported downstream. However, RT suggests that this result is strongly dependent on the hydraulic connectivity between both aquifers. As the reduction from Cr(VI) to Cr(III) progresses, concentrations of Cr(III) are strongly controlled by the equilibrium with $Cr(OH)_3$(am).

Uncertainty quantification analysis suggests that Cr(VI) concentrations in the deep aquifer are sensitive to physical and geochemical parameters. As regards the physical parameters, they are strongly sensitive to hydraulic conductivity of the AQT unit because it mainly controls the hydraulic connectivity between both Pampeano and Puelche aquifers. When it comes to the geochemical parameters, Cr(VI) concentrations in the PUAQ are sensitive to organic matter contents and reduction rates of Cr(VI) to Cr(III).

As regards the temporal evolution of the Cr concentrations in both aquifers, it is important to point out that the Cr(VI) source term is treated here as a constant one, and it could not be realistic with the present-day conditions of the real system. Other implications about the evolution of the contamination could be derived based on Cr field measurements and modelling results described here. The first one highlights the relevance to experimentally assess the natural attenuation as a viable option in this system. It could be conducted through batch experiments on natural sediments to assess their capacity to induce the Cr(VI) reduction to Cr(III). The second one highlights the relevance to increase the characterisation of the Cr(VI) source term in two main aspects, the physical location and mass loading.

References

Bain, J.G., Mayer, K.U., Molson, J.W.H., Blowes, D.W., Frind, E.O., Kahnt, R. and Jenk, U. (2001) 'Assessment of the suitability of reactive transport modeling for the evaluation of mine closure options', *Journal of Contaminant Hydrology*, Vol. 52, pp.109–135.

Bea, S.A., Mayer, K.U. and MacQuarrie, K.T.B. (2016) 'Reactive transport and thermo-hydro-mechanical coupling in deep sedimentary basins affected by glaciation cycles: model development, verification and illustrative example', *Geofluids*, Vol. 16, No. 2, pp.279–300.

Bea, S.A., Wainwright, H., Spycher, N., Faybishenko, B., Hubbard, S.S. and Denham, M.E. (2013) 'Identifying key controls on the behavior of an acidic-U(VI) plume in the Savannah River Site using reactive transport modeling', *Journal of Contaminant Hydrology*, Vol. 151, pp.34–54.

Bea, S.A., Wilson, S., Mayer, K.U., Dipple, G., Power, I. and Gamazo, P. (2012) 'Reactive transport modeling of natural carbon sequestration in ultramafic mine tailings', *Vadose Zone Journal*, Vol. 11, No. 2, pp.1–17.

Blowes, D. (2002) 'Tracking hexavalent Cr in groundwater', *Science*, Vol. 295, pp.2024–2025.

Brookfield, A., Blowes, D.W. and Mayer, K.U. (2006) 'Integration of field measurements and reactive transport modelling to evaluate contaminant transport at a sulfide mine tailings impoundment', *Journal of Contaminant Hydrology*, Vol. 88, pp.1–22.

Cacuci, D.G. (2003) *Sensitivity and Uncertainty Analysis*, Vol. 1: Theory, Chapman and Hall/CRC Press, Boca Raton, FL.

Doherty, J. (2008) *PEST: Model-Independent Parameter Estimation. Watermark Numerical Computing*, Brisbane, Australia, http://pesthomepage. org/ (2008)

Economou-Eliopoulos, M., Megremi, I. and Vasilatos, C. (2011) Factors controlling the heterogeneous distribution of Cr(VI) in soil, plants and groundwater: evidence from the Assopos basin, Greece', *Chemie der Erde-Geochemistry*, Vol. 71, pp.39–52.

Finsterle, S. (2010) *ITOUGH2 User's Guide, Report LBNL-40040*, Lawrence Berkeley National Laboratory, Berkeley, Calif.

Gerard, F., Mayer, K.U., Hodson, M.J. and Ranger, J. (2008) 'Modelling the biogeochemical cycle of silicon in soils: application to a temperate forest ecosystem', *Geochimica et Cosmochimica Acta*, Vol. 72, pp.741–758.

Jamieson-Hanes, J., Gibson, B., Lindsay, M., Kim, Y., Ptacek, C. and Blowes, D. (2012) 'Chromium isotope fractionation during reduction of Cr(VI) under saturated flow conditions', *Environmental Science and Technology*, Vol. 46, pp.6783–6789.

Kotas, J. and Stasicka, Z. (2000) 'Chromium occurrence in the environment and methods of its speciation', *Environ. Pollut.*, Vol. 107, pp.263–283.

Mayer, K.U., Benner, S. and Blowes, D. (2006) 'Process-based reactive transport modeling of a permeable reactive barrier for the treatment of mine drainage', *Journal of Contaminant Hydrology*, Vol. 85, pp.195–211.

Mayer, K.U., Blowes, D.W. and Frind, E.O. (2001) 'Reactive transport modeling of an in situ reactive barrier for the treatment of hexavalent chromium and trichloroethylene in groundwater', *Water Resources Research*, Vol. 37, pp.3091–3103.

Mayer, K.U., Frind, E.O. and Blowes, D.W. (2002) 'Multicomponent reactive transport modeling in variably saturated porous media using a generalized formulation for kinetically controlled reactions', *Water Resources Research*, Vol. 38, No. 1174.

Melián, A.F. (2014) *Actualización del modelo numérico de flujo de agua subterránea en la cuenca Matanza-Riachuelo (Buenos Aires, Argentina) (MSc thesis) Fundación Centro Internacional de Hidrología Subterránea*, Universitat Politècnica de Catalunya, p.149. Unpublished.

Morris, M.D. (1991) 'Factorial sampling plans for preliminary computational experiments', *Technometrics*, Vol. 33, pp.161–174.

Palmer, C.D. and Wittbrodt, P.R. (1991) 'Processes affecting the remediation of chromium contaminated sites', *Environ. Health Perspectives*, Vol. 92, pp.25–40.

Parkhurst, D. and Appelo, C. (2013) *User's Guide to PHREEQC, A Computer Program for Speciation, Batch-Reaction, One-Dimensional Transport and Inverse Geochemical Calculations*, US Geological Survey Water-Resources Investigations Report 99-4259.

Rai, D., Eary, L.E. and Zachara, J.M. (1989) 'Environmental chemistry of chromium', *Science of the Total Environment*, Vol. 86, pp.15–23.

Salvador, C. (2013) *Historia de la Industria Curtidora Argentina*, Ed. Dunken, p.320.

Spiessl, S., MacQuarrie, K.T.B. and Mayer, K.U. (2008) 'Identification of key parameters controlling dissolved oxygen migration and attenuation in fractured crystalline rocks', *Journal of Contaminant Hydrology*, Vol. 95, pp.141–153.

Steefel, C.I., DePaolo, D.J. and Lichtner, P.C. (2005) 'Reactive transport modeling: An essential tool and a new research approach for the Earth sciences', *Earth and Planetary Science Letters*, Vol. 240, pp.539–558.

Wanner, C., Eggenberger, U. and Mäder, U. (2012) 'A chromate-contaminated site in southern Switzerland – Part 2: Reactive transport modeling to optimize remediation options', *Applied Geochemistry*, Vol. 27, pp.655–662.

Watson, I.A., Oswald, S.E., Mayer, K.U., Wu, Y. and Banwart, S.A. (2003) 'Modeling kinetic processes controlling hydrogen and acetate concentrations in an aquifer-derived microcosm', *Environmental Science & Technology*, Vol. 37, pp.3910–3919.

Xie, M., Mayer, K., Claret, F., Alt-Epping, P., Jacques, D., Steefel, C., Chiaberge, C. and Simunek, J. (2014) 'Implementation and evaluation of permeability-porosity and tortuosity-porosity relationships linked to mineral dissolution-precipitation', *Computational Geosciences*, pp.1–17.

Zabala, M.E., Manzano, M. and Vives, L. (2016) 'Groundwater chemical baseline values to assess the recovery plan in the Matanza-Riachuelo River basin Argentina', *Science of the Total Environment*, Vol. 541, pp.1516–1530.